# Synthesis and Evaluation of a Novel Hydroxamate Based Fluorescent Photoprobe for Imaging of Matrix Metalloproteinases

**ARTICLE** *in* BIOCONJUGATE CHEMISTRY · MAY 2009

Impact Factor: 4.51 · DOI: 10.1021/bc8004478 · Source: PubMed



**11 AUTHORS**, INCLUDING:

Andreas Faust
University of Münster
**53** PUBLICATIONS **602** CITATIONS
SEE PROFILE

Jens Waldeck
University of Münster
**22** PUBLICATIONS **298** CITATIONS
SEE PROFILE

Carsten Höltke
University of Münster
**45** PUBLICATIONS **579** CITATIONS
SEE PROFILE

Walter Heindel
University of Münster
**275** PUBLICATIONS **7,983** CITATIONS
SEE PROFILE

# Synthesis and Evaluation of a Novel Hydroxamate Based Fluorescent Photoprobe for Imaging of Matrix Metalloproteinases

Andreas Faust,*[,†,‡,||,⊥] Bianca Waschkau,[†,⊥] Jens Waldeck,[†] Carsten Höltke,[†,‡,||] Hans-Jörg Breyholz,[‡,||] Stefan Wagner,[‡,||] Klaus Kopka,[‡,||] Otmar Schober,[‡,||] Walter Heindel,[†] Michael Schäfers,[‡,§,||] and Christoph Bremer[†,§,||]

Department of Clinical Radiology, Albert-Schweitzer-Strasse 33, University Hospital Münster, 48149 Münster, Germany, Department of Nuclear Medicine, Albert-Schweitzer-Strasse 33, University Hospital Münster, 48149 Münster, Germany, Interdisciplinary Center for Clinical Research (IZKF Münster), Domagkstr. 3, University of Münster, 48149 Münster, Germany, and European Institute for Molecular Imaging (EIMI), University of Münster, Mendelstr. 11, 48149 Münster, Germany. Received October 20, 2008; Revised Manuscript Received March 11, 2009

The assessment of matrix metalloproteinase (MMP) activity in vivo is highly desirable in various human diseases such as cancers. Hydroxamic acids based on CGS27023A or CGS25966 are nonpeptidyl lead structures that specifically target activated MMPs in vivo. The aim of this study was the modification and fluorescent labeling of these lead structures to develop a highly affine, nonpeptide MMP inhibitor (MMPI)-ligand for molecular optical imaging of activated MMPs. An 11 step synthesis was developed involving a PEGylated benzyl derivative as a spacer to minimize the interactions between the activated MMP and the dye of conjugate **11** with an azide as a protected amino function. After reducing the azide (Staudinger reaction) and labeling with Cy5.5, we obtained a CGS-based MMP inhibitor **11** with a fluorescent signaling flag. To evaluate the biological properties of this photoprobe, three human cancer cell lines (A-673, HT-1080 and BT-20) were characterized with respect to their MMP-2 and -9 (gelatinases) expression levels (real-time PCR) and protein levels (Western blotting). Initially, fluorogenic inhibition assays were used to assess the MMP inhibition potential. The PEGylated CGS **10** showed complete inhibition of MMP-2 and MMP-9 activities in vitro both for purified MMP-2/-9 (active and pro-forms) and MMP-2/-9 containing cell culture supernatants. To test the imaging potential in biological tissues, gelatinase activity was measured on tumor cryostat sections of the above-mentioned tumor cells using FITC-labeled dye-quenched gelatin. Gelatinase positive tumors revealed strong binding of CGS-Cy5.5 **11**, while gelatinase negative tumors were not targeted. In conclusion, this new CGS-based MMP photoprobe has a high affinity for MMP-2 and -9 and is thus a promising candidate for sensitive imaging of MMP activity in various diseases in patients.

## INTRODUCTION

Matrix metalloproteinases (MMPs) are a family of currently more than 24 known mammalian emzymes, which are able to degrade structural components of the extracellular matrix (ECM) and basement membranes with overlapping substrate specificities (*1*−*3*). On the basis of their specificity, the MMPs are classified into collagenases, gelatinases, stromelysins, and matrilysins. (*4*) MMPs are secreted as inactive pro-enzymes (zymogens). A mechanism termed cysteine switch (*5*) initiates the activation of the MMPs, which are subsequently tightly controlled by several endogenous inhibitors, e.g., the plasma inhibitor α2-macroglobulin and the four tissue inhibitors of metalloproteinases (TIMPs) (*6*). MMPs and TIMPs participate in physiological tissue remodelling processes that require the disruption of ECM barriers to allow cell migration and the modification of the matrix microenvironment. Elevated MMP expression and activity has been found in numerous human diseases, including inflammatory processes, cancer, and atherosclerosis (*7, 8*). Especially, MMP-2 and -9 play a crucial role in local and metastatic invasion of cancer. One of the earliest events in the metastatic spread of cancer is the invasion through the basement membrane and proteolytic degradation of the extracellular matrix proteins, such as, collagens, laminin, elastin and fibronectin, etc., and nonmatrix proteins. MMPs are thus important regulators of tumor growth, both at the primary site and in distant metastases. Given that MMPs are clearly implicated in many human cancers, these represent important targets for imaging tumor biology (*9, 10*).

**Scheme 1. Structures of CGS25966 (A) and CGS27023A (B)**

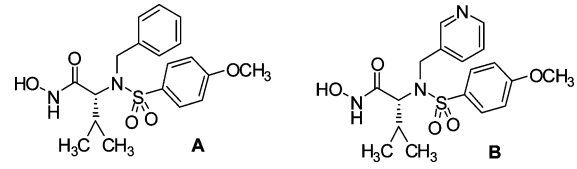


In this study, the synthesis of a MMP ligand based on the broad-spectrum inhibitor lead structures CGS27023A and CGS25966 (Scheme 1) is described. A polyethylene glycol (PEG) spacer group containing the amino functionality was successfully inserted to enable labeling with fluorescent dyes without significantly changing the MMP binding potential. The conjugation of the fluorescent dye Cy5.5 was accomplished by forming an amide bond under standard conditions. Enzyme activity assays, blocking experiments with the unlabeled CGS

* To whom correspondence should be addressed. Department of Clinical Radiology, Albert-Schweitzer-Str. 33, University Hospital Münster, 48149 Münster, Germany. Tel: +49-251-8347362. Fax: +49-251-8347363. E-mail: faustan@uni-muenster.de.

† Department of Clinical Radiology, University Hospital Münster.

‡ Department of Nuclear Medicine, University Hospital Münster.

§ Interdisciplinary Center for Clinical Research (IZKF Münster), University of Münster.

⊥ These authors contributed equally to this work.

|| European Institute for Molecular Imaging (EIMI), University of Münster.

10.1021/bc8004478 CCC: $40.75 
Published on Web 04/17/2009

**10**, and in vitro binding studies with CGS-Cy5.5 **11** confirmed a high binding potential of the probe to the target proteins.

## EXPERIMENTAL PROCEDURES

**Materials and Methods.** All chemicals, reagents, and solvents for the synthesis of the compounds were of analytical grade and were purchased from commercial sources. For the labeling procedure, DNA-grade dimethylformamide was used. Melting points (uncorrected) were determined on a Stuart Scientific SMP3 capillary melting point apparatus. $^1$H NMR and $^{13}$C NMR spectra were recorded on a Bruker ARX 300 (Bruker BioSpin GmbH, Rheinstetten, Germany). Mass spectrometry was performed using a QUATTRO LCZ (Waters Micromass, Manchester, UK) spectrometer with a nanospray capillary inlet.

**Synthetic Organic Chemistry.** *Tetraethyleneglycol Dimethanesulfonate.* Methanesulfonyl chloride (317 mL, 470 g, 4.1 mol) was added dropwise over a period of 4 h to a solution of tetraethylene glycol (347 mL, 388 g, 2 mol) in dichloromethane (1.8 L) and triethyl amine (570 mL, 415 g, 4.1 mol) at 0 °C. The mixture was stirred at ambient temperature for an additional 16 h, and the resulting precipitate was filtered off. Concentration of the filtrate yielded an orange oil, which was used without further purification. Yield: 596 g (1.7 mol, 85%). $^1$H NMR ($CDCl_3$, 300 MHz): $\delta$ (ppm) = 3.08 (s, 6H, $SO_3CH_3$), 3.65−3.68 (m, 8H, $OCH_2CH_2O$), 3.76−3.78 (m, 4H, $SO_3CH_2CH_2$), 4.37−4.40 (m, 4H, $SO_3CH_2CH_2$). $^{13}$C NMR ($CDCl_3$, 75 MHz): $\delta$ (ppm) = 37.6 ($SO_3CH_3$), 68.9 ($SO_3CH_2CH_2$), 69.2 ($SO_3CH_2CH_2$), 70.4, 70.5 ($OCH_2CH_2O$). MS ($ES^+$) *m/e* = 373.1 $(M + Na)^+$, 351.1 $(M + H)^+$.

*2-(2-(2-(2-Azidoethoxy)ethoxy)ethoxy)ethyl Methanesulfonate (**1**).* To a solution of the dimesylate (83.4 g, 272 mmol) in dimethyl formamide (600 mL) sodium azide (10.6 g, 163 mmol) was added, and the reaction mixture was stirred at 120 °C for 5 h. Most of the dimethyl formamide was removed in vacuo. The crude product was dissolved in ethyl acetate (400 mL) and washed with water (5 × 200 mL) and brine (200 mL) and dried over magnesium sulfate. After removing the solvent, the resulting oil was chromatographed on a silica gel column (cyclohexane/EtOAc 2/1 to 1/1) to give a light yellow oil. Yield: 17.2 g (58 mmol, 36%). $^1$H NMR ($CDCl_3$, 300 MHz): $\delta$ (ppm) = 3.08 (s, 3H, $SO_3CH_3$), 3.64−3.69 and 3.76−3.79 (m, 14H, $OCH_2CH_2O$ and $OCH_2CH_2N_3$), 4.37−4.40 (m, 2H, $SO_3CH_2CH_2$). $^{13}$C NMR ($CDCl_3$, 75 MHz): $\delta$ (ppm) = 37.6 ($SO_3CH_3$), 51.0 ($CH_2N_3$), 68.8 ($SO_3CH_2CH_2$), 69.3 ($SO_3CH_2CH_2$), 69.9, 70.4, 70.5 ($OCH_2CH_2O$). MS ($ES^+$) *m/e* = 319.1 $(M + Na)^+$, 297.1 $(M + H)^+$.

*4-(2-(2-(2-(2-Azidoethoxy)ethoxy)ethoxy)ethoxy)benzaldehyde (**2**).* To a solution of 14.2 g (47.8 mmol) of methansulfonate **1** and 9.16 g (75 mmol) of 4-hydroxybenzaldehyde in 200 mL of dimethyl formamide, 49 g (150 mmol) of cesium carbonate was added, and the resulting suspension was stirred at 100 °C for 2 h. After cooling to room temperature, 400 mL of ethyl acetate and 400 mL of water were added, and the organic layer was extracted with 1 N NaOH (150 mL) three times. After washing with water (3 × 150 mL) and brine, drying over magnesium sulfate, and removing the solvent, the crude product was chromatographed on a silica gel column (toluene/acetone 10/1) to give a yellow oil. Yield: 11.6 g (36 mmol; 75%). $^1$H NMR ($CDCl_3$, 300 MHz): $\delta$ (ppm) = 3.36−3.39 (m, 2H, $OCH_2CH_2N_3$), 3.65−3.74 (m, 10H, $OCH_2CH_2O$), 3.87−3.90 (m, 2H, $PhOCH_2CH_2$), 4.20−4.23 (m, 2H, $PhOCH_2CH_2$), 7.02 (d, 2H, Ph*H*, $^3J_{HH}$ = 7.5 Hz), 7.82 (d, 2H, Ph*H*, $^3J_{HH}$ = 7.5 Hz). $^{13}$C NMR ($CDCl_3$, 75 MHz): $\delta$ (ppm) = 50.5 ($CH_2N_3$), 67.6, 69.3, 69.9, 70.5, 70.6, 70.7 ($OCH_2CH_2O$), 114.7 (Ph*C*H), 125.2 (q-Ph*C*CHO), 131.8 (Ph*C*H), 163.7 (qPh*C*O), 190.7 (Ph*C*HO). HRMS ($ES^+$): calcd. ($C_{15}H_{21}N_3O_5Na$) = 346.1373; found = 346.1379.

*(4-(2-(2-(2-(2-Azidoethoxy)ethoxy)ethoxy)ethoxy)phenyl)methanol (**3**).* To a solution of 4-(2-(2-(2-(2-azidoethoxy)ethoxy)ethoxy)-ethoxy)benzaldehyde **2** (26.47 g, 82 mmol) in 300 mL of methanol, sodiumborhydride (4.65 g, 123 mmol) was carefully added at 0 °C. After stirring for 2 h at 0 °C, the excess sodiumborhydride was destroyed by adding 1 N HCl. The solvent was removed, and the resulting crude product was chromatographed on a silica gel column (cyclohexane/ethyl acetate 1/1) to give a colorless viscous oil. Yield: 23.66 g (73 mmol; 89%). $^1$H NMR ($CDCl_3$, 300 MHz): $\delta$ (ppm) = 2.11 (bs, 1H, O*H*), 3.34−3.37 (m, 2H, $OCH_2CH_2N_3$), 3.63−3.72 (m, 10H, $OCH_2CH_2O$), 3.83−3.86 (m, 2H, $PhOCH_2CH_2$), 4.11−4.13 (m, 2H, $PhOCH_2CH_2$), 4.58 (s, 2H, $CH_2OH$), 6.87 (d, 2H, Ph*H*, $^3J_{HH}$ = 7.2 Hz), 7.26 (d, 2H, Ph*H*, $^3J_{HH}$ = 7.2 Hz). $^{13}$C NMR ($CDCl_3$, 75 MHz): $\delta$ (ppm) = 50.5 ($CH_2N_3$), 64.7 ($PhCH_2OH$), 67.4, 69.6, 69.9, 70.5, 70.7 ($OCH_2CH_2O$), 114.5 (Ph*C*H), 128.4 (q-Ph*C*CHO), 133.3 (Ph*C*H), 158.2 (qPh*C*O). HRMS ($ES^+$): calcd. ($C_{15}H_{23}N_3O_5Na$) = 348.1530; found = 348.1522.

*4-(2-(2-(2-(2-Azidoethoxy)ethoxy)ethoxy)ethoxy)benzyl-2,2,2-trifluoro-acetate (**4**).* Benzylalcohol **3** (8.5 g, 26.2 mmol) was dissolved in dry tetrahydrofurane (50 mL), and trifluoroacetic acid anhydride (6.83 g, 4.5 mL, 32.5 mmol) was added slowly with stirring, and the mixture was heated to reflux for 30 min. After cooling to room temperature, the mixture was diluted with diethyl ether (150 mL) and washed with saturated $NaHCO_3$. The ether layer was dried with magnesium sulfate and concentrated to give a light yellow oil. Yield: 10.48 g (25 mmol, 95%). $^1$H NMR ($CDCl_3$, 300 MHz): $\delta$ (ppm) = 3.35−3.38 (m, 2H, $OCH_2CH_2N_3$), 3.63−3.73 (m, 10H, $OCH_2CH_2O$), 3.85−3.88 (m, 2H, $PhOCH_2CH_2$), 4.14−4.16 (m, 2H, $PhOCH_2CH_2$), 5.28 (s, 2H, $CH_2OCOCF_3$), 6.93 (d, 2H, Ph*H*, $^3J_{HH}$ = 7.2 Hz), 7.31 (d, 2H, Ph*H*, $^3J_{HH}$ = 7.2 Hz). $^{13}$C NMR ($CDCl_3$, 75 MHz): $\delta$ (ppm) = 50.5 ($CH_2N_3$), 67.4 ($PhCH_2O$), 69.5, 69.8, 70.5, 70.7 ($OCH_2CH_2O$), 114.4 ($COCF_3$, $^1J_{CF}$ = −284 Hz), 114.7 (Ph*C*H), 125.4 (q-Ph*C*CHO), 130.5 (Ph*C*H), 157.3 ($COCF_3$, $^2J_{CF}$ = −42 Hz), 159.5 (qPh*C*O). $^{19}$F-NMR ($CDCl_3$, 282 MHz): $\delta$ (ppm) = −75.1 ($CF_3$). HRMS ($ES^+$): calcd. ($C_{17}H_{22}F_3N_3O_6Na$) = 444.1358; found = 444.1355.

*1-(2-(2-(2-(2-Azidoethoxy)ethoxy)ethoxy)ethoxy)-4-(bromomethyl)benzene (**5**).* Benzyl trifluoroacetate **4** (10.4 g, 25 mmol) was dissoled in dry tetrahydrofurane (50 mL), and dry lithium bromide (2.75 g, 32 mmol) was added with stirring. The mixture was heated to reflux for 20 h. After removing the solvent, the dark brown oil was chromatograhed on a silica gel column (cyclohexane/ethyl acetate 1/1) to give yellow oil. Yield: 8.4 g (21.6 mmol, 87%). $^1$H NMR ($CDCl_3$, 300 MHz): $\delta$ (ppm) = 3.34−3.38 (m, 2H, $OCH_2CH_2N_3$), 3.62−3.71 (m, 10H, $OCH_2CH_2O$), 3.83−3.86 (m, 2H, $PhOCH_2CH_2$), 4.10−4.13 (m, 2H, $PhOCH_2CH_2$), 4.49 (s, 2H, $CH_2Br$), 6.87 (d, 2H, Ph*H*, $^3J_{HH}$ = 7.2 Hz), 7.30 (d, 2H, Ph*H*, $^3J_{HH}$ = 7.2 Hz). $^{13}$C NMR ($CDCl_3$, 75 MHz): $\delta$ (ppm) = 50.5 ($CH_2N_3$), 33.8 ($PhCH_2Br$), 67.3, 69.5, 69.8, 70.3, 70.5, 70.7 ($OCH_2CH_2O$), 114.7 (Ph*C*H), 129.9 (q-Ph*C*CHO), 130.3 (Ph*C*H), 158.7 (qPh*C*O). HRMS ($ES^+$): calcd. ($C_{15}H_{22}BrN_3O_4Na$) = 410.0686, 411.0716, 412.0667, 413.0696; found = 410.0690, 411.0721, 412.0671, 413.0702.

*(R)-Methyl-2-(4-methoxyphenylsulfonamido)-3-methylbutanoate (**6**).* A solution of D-valine methylester (12.56 g, 75 mmol) in 35 mL of pyridine was cooled to 0 °C and 4-methoxybenzylsulfonyl chloride (15.5 g, 75 mmol) was slowly added. The resulting solution was stirred for 2 days at room temperature while a precipitate was formed. The suspension was diluted with 200 mL of dichloromethane and washed with 1 N HCl (200 mL), water (3 × 150 mL), and brine. After drying over magnesium sulfate, the solvent was removed to give the desired product with sufficient purity. Yield: 21.4 g (71 mmol, 95%). $^1$H NMR ($CDCl_3$, 300 MHz): $\delta$ (ppm) = 0.87 (d, 3H, $CH(CH_3)_2$, $^3J_{HH}$ = 6.8 Hz), 0.94 (d, 3H, $CH(CH_3)_2$, $^3J_{HH}$ = 6.8

Hz), 1.97−2.08 (m, 1H, C*H*($CH_3$)$_2$), 3.47 (s, 3H, COOC$H_3$), 3.70 (dd, 1H, (COO)C*H*, $^3J_{HH}$ = 5.2 Hz and 10.2 Hz), 3.86 (s, 3H, PhOC$H_3$), 5.20 (d, 1H, N*H*, $^3J_{HH}$ = 10.2 Hz), 6.96 (d, 2H, Ph*H*, $^3J_{HH}$ = 9 Hz), 7.76 (d, 2H, Ph*H*, $^3J_{HH}$ = 9 Hz). $^{13}$C NMR ($CDCl_3$, 75 MHz): $\delta$ (ppm) = 17.4, 18.9 (CH($CH_3$)$_2$), 31.5 (*C*H($CH_3$)$_2$), 52.2 (COO*C*H$_3$), 55.6 (PhO*C*H$_3$), 60.9 (COO*C*H), 114.0 (Ph*C*H), 129.4 (Ph*C*H), 131.1 (qPh*C*SO$_2$), 162.9 (qPh-*C*OCH$_3$), 171.8 (*C*OOCH$_3$). HRMS (ES$^+$): calcd. ($C_{12}H_{17}NO_5SNa$) = 310.0720; found = 310.0721.

*(R)-Methyl-2-(N-(4-(2-(2-(2-(2-azidoethoxy)ethoxy)ethoxy)ethoxy)-benzyl)-4-methoxyphenyl-sulfonamido)-3-methylbutanoate (***7***).* To a solution of (*R*)-methyl-2-(4-methoxyphenyl-sulfonamido)-3-methyl-butanoate **6** (3.1 g, 10.1 mmol) and 1-(2-(2-(2-(2-azidoethoxy)-ethoxy)ethoxy)ethoxy)-4-(bromomethyl)benzene **5** (4 g, 10.3 mmol) in 100 mL of butanone potassium carbonate (7 g, 50 mmol) was added, and the resulting suspension was stirred for 4 h at 60 °C. After removing the solvent, the crude product was diluted with dichloromethane (150 mL) and washed with water (3 × 150 mL) and brine. The solution was dried over magnesium sulfate, filtered, and chromatographed on a silica gel column (cyclohexane/ethyl acetate 3/2) to give a colorless viscous oil. Yield: 4.56 g (7.5 mmol, 73%). $^1$H NMR ($CDCl_3$, 300 MHz): $\delta$ (ppm) = 0.75 (d, 3H, CH(C$H_3$)$_2$, $^3J_{HH}$ = 6.5 Hz), 0.80 (d, 3H, CH(C$H_3$)$_2$, $^3J_{HH}$ = 6.5 Hz), 1.89−1.97 (m, 1H, C*H*($CH_3$)$_2$), 3.41 (s, 3H, COOC$H_3$), 3.37−3.41 (m, 2H, OCH$_2$C$H_2$N$_3$), 3.66−3.73 (m, 11H, OC$H_2$C$H_2$O, COOC*H*), 3.84−3.88 (m, 5H, PhOCH$_2$C$H_2$, PhOC$H_3$), 4.09−4.12 (m, 2H, PhOC$H_2$CH$_2$), 4.33 (AB, 1H, $^2J_{HH}$ = 11.8 Hz, PhC$H_2$), 4.58 (AB, 1H, $^2J_{HH}$ = 11.8 Hz, PhC$H_2$), 6.80 (d, 2H, $^3J_{HH}$ = 8.6 Hz, Ph*H*), 6.91 (d, 2H, $^3J_{HH}$ = 8.9 Hz, Ph*H*), 7.30 (d, 2H, $^3J_{HH}$ = 8.6 Hz, Ph*H*), 7.69 (d, 2H, $^3J_{HH}$ = 8.9 Hz, Ph*H*). $^{13}$C NMR ($CDCl_3$, 75 MHz): $\delta$ (ppm) = 19.6 (CH(*C*H$_3$)$_2$), 28.5 (*C*H-($CH_3$)$_2$), 48.2 (N*C*H$_2$Ph), 50.7 (*C*H$_2$N$_3$), 51.4 (COO*C*H$_3$), 55.6 (PhO*C*H$_3$), 66.1 (COO*C*H), 67.4 (PhO*C*H$_2$), 69.8, 70.0, 70.7, 70.8, 70.9 (O*C*H$_2$*C*H$_2$O), 113.7, 114.1 (Ph*C*H), 129.4, 129.5, 130.1 (q-Ph*C*CH$_2$, Ph*C*H), 131.9 (q-Ph*C*SO$_2$), 158.1, 162.6 (qPh*C*O), 170.8 (*C*OO). HRMS (ES$^+$): calcd. ($C_{28}H_{40}N_4O_9SNa$) = 631.2414; found = 631.2416.

*(R)-2-(N-(4-(2-(2-(2-(2-Azidoethoxy)ethoxy)ethoxy)ethoxy)benzyl)-4-methoxyphenylsulfon-amido)-3-methylbutanoic acid (***8***).* To a solution of the methyl ester **7** in tetrahydrofuran, methanol and water (8:1:1, 100 mL) lithium hydroxide (2.4 g, 100 mmol) was added, and the resulting suspension was stirred at room temperature for 2 days. After removing the solvent, the crude product was purified on a silica gel column (cyclohexane/ethyl acetate 2/1 with 2.5% acetic acid) to give a colorless sticky oil. Yield: 9.1 g (15.3 mmol, 78%). $^1$H NMR ($CDCl_3$, 300 MHz): $\delta$ (ppm) = 0.75 (d, 3H, CH(C$H_3$)$_2$, $^3J_{HH}$ = 6.5 Hz), 0.89 (d, 3H, CH(C$H_3$)$_2$, $^3J_{HH}$ = 6.5 Hz), 1.92−2.00 (m, 1H, C*H*($CH_3$)$_2$), 3.36−3.40 (m, 2H, OCH$_2$C$H_2$N$_3$), 3.66−3.71 (m, 11H, OC$H_2$C$H_2$O, COOC*H*), 3.84−3.88 (m, 5H, PhOCH$_2$C$H_2$, PhOC$H_3$), 4.09−4.14 (m, 2H, PhOC$H_2$CH$_2$), 4.38 (AB, 1H, $^2J_{HH}$ = 15.7 Hz, PhC$H_2$), 4.58 (AB, 1H, $^2J_{HH}$ = 15.7 Hz, PhC$H_2$), 6.79 (d, 2H, $^3J_{HH}$ = 8.6 Hz, Ph*H*), 6.89 (d, 2H, $^3J_{HH}$ = 8.9 Hz, Ph*H*), 7.27 (d, 2H, $^3J_{HH}$ = 8.6 Hz, Ph*H*), 7.71 (d, 2H, $^3J_{HH}$ = 8.9 Hz, Ph*H*), 10.53 (bs, 1H, COO*H*). $^{13}$C NMR ($CDCl_3$, 75 MHz): $\delta$ (ppm) = 19.7 (CH(*C*H$_3$)$_2$), 28.3 (*C*H($CH_3$)$_2$), 48.4 (N*C*H$_2$Ph), 50.6 (*C*H$_2$N$_3$), 55.6 (PhO*C*H$_3$), 66.0 (COO*C*H), 67.3 (PhO*C*H$_2$), 69.7, 70.0, 70.6, 70.7, 70.8 (O*C*H$_2$*C*H$_2$O), 113.8, 114.1 (Ph*C*H), 129.1 (q-Ph*C*CH$_2$), 129.6, 130.2 (Ph*C*H), 131.6 (q-Ph*C*SO$_2$), 158.1, 162.7 (qPh*C*O), 175.1 (*C*OOH). HRMS (ES$^+$): calcd. ($C_{27}H_{38}N_4O_9SNa$) = 617.2252; found = 617.2259.

*(R)-2-(N-(4-(2-(2-(2-(2-Azidoethoxy)ethoxy)ethoxy)ethoxy)benzyl)-4-methoxyphenylsulfon-amido)-N-hydroxy-3-methylbutanamide (***9***).* A suspension of *N*-hydroxy-2-pyridone (500 mg, 4.5 mmol) in dichloromethane (25 mL) was subsequently treated at room temperature with acid **8** (1.8 g, 3 mmol) and 2-morpholinoethyl isocyanide (631 mg, 0.62 mL, 4.5 mmol). Stirring was continued for 19 h after which time the formation of the intermediate pyridine active ester was complete. The solution was treated at 0 °C with TMSO-NH$_2$ (473 mg, 0.56 mL, 4.5 mmol), and stirring was continued at 0 °C for 7 h. The solution was washed with saturated aqueous $NaHCO_3$ (75 mL) and water (3 × 75 mL). The aqueous layer was additionally washed with dichloromethane (100 mL), and the combined organic layers were dried over magnesium sulfate and subsequently filtered. The crude product was chromatographed on a silica gel column (cyclohexane/ethyl acetate 1/1 → 1/4) to give a colorless and highly viscous oil. Yield: 930 mg (1.53 mmol, 51%). $^1$H NMR ($CDCl_3$, 300 MHz): $\delta$ (ppm) = 0.50 (d, 3H, CH(C$H_3$)$_2$, $^3J_{HH}$ = 6.5 Hz), 0.79 (d, 3H, CH(C$H_3$)$_2$, $^3J_{HH}$ = 6.5 Hz), 2.10−2.15 (m, 1H, C*H*($CH_3$)$_2$), 3.37−3.40 (m, 2H, OCH$_2$C$H_2$N$_3$), 3.66−3.75 (m, 11H, OC$H_2$C$H_2$O, C*H*CON), 3.84−3.89 (m, 5H, PhOCH$_2$C$H_2$, PhOC$H_3$), 4.09−4.12 (m, 2H, PhOC$H_2$CH$_2$), 4.45 (AB, 1H, $^2J_{HH}$ = 15.4 Hz, PhC$H_2$), 4.57 (AB, 1H, $^2J_{HH}$ = 15.4 Hz, PhC$H_2$), 6.79 (d, 2H, $^3J_{HH}$ = 8.6 Hz, Ph*H*), 6.88 (d, 2H, $^3J_{HH}$ = 8.9 Hz, Ph*H*), 7.27 (d, 2H, $^3J_{HH}$ = 8.6 Hz, Ph*H*), 7.61 (d, 2H, $^3J_{HH}$ = 8.9 Hz, Ph*H*), 9.36 (bs, 1H, CON*H*OH). $^{13}$C NMR ($CDCl_3$, 75 MHz): $\delta$ (ppm) = 19.2, 19.8 (CH(*C*H$_3$)$_2$), 27.3 (*C*H($CH_3$)$_2$), 48.0 (N*C*H$_2$Ph), 50.7 (*C*H$_2$N$_3$), 55.6 (PhO*C*H$_3$), 63.7 (NHCO*C*H), 67.4 (PhO*C*H$_2$), 69.7, 70.0, 70.6, 70.7, 70.8 (O*C*H$_2$*C*H$_2$O), 114.1, 114.2 (Ph*C*H), 129.0 (q-Ph*C*CH$_2$), 129.4, 130.5 (Ph*C*H), 131.7 (q-Ph*C*SO$_2$), 158.2, 162.9 (qPh*C*O), 167.2 (*C*ONHOH). HRMS (ES$^+$): calcd. ($C_{27}H_{39}N_5O_9SNa$) = 632.2361; found = 632.2360.

*(R)-2-(N-(4-(2-(2-(2-(2-aminoethoxy)ethoxy)ethoxy)ethoxy)benzyl)-4-methoxyphenylsulfon-amido)-N-hydroxy-3-methylbutanamide (***10***).* To a solution of the hydroxamic acid **9** (900 mg, 1.48 mmol) in THF (50 mL) was added at room temperature triphenylphosphine (500 mg, 1.9 mmol), and stirring was continued for 16 h. The solution was treated with water (34 $\mu$L, 1.9 mmol), and after stirring for an additional 3 h, the solvent was removed. The crude product was chromatographed on a silica gel column (ethyl acetate/methanol 2/1 with 2% triethylamine) to give colorless foam. Yield: 410 mg (0.7 mmol, 47%). $^1$H NMR ($CDCl_3$, 300 MHz): $\delta$ (ppm) = 0.54 (d, 3H, CH(C$H_3$)$_2$, $^3J_{HH}$ = 6.5 Hz), 0.81 (d, 3H, CH(C$H_3$)$_2$, $^3J_{HH}$ = 6.5 Hz), 2.16−2.18 (m, 1H, C*H*($CH_3$)$_2$), 3.45−3.87 (m, 18H, PEG-C$H_2$, C*H*CON, PhOC$H_3$), 4.07−4.09 (m, 2H, PhOC$H_2$CH$_2$), 4.40 (AB, 1H, $^2J_{HH}$ = 15.4 Hz, PhC$H_2$), 4.65 (AB, 1H, $^2J_{HH}$ = 15.4 Hz, PhC$H_2$), 6.41 (bs, 2H, N$H_2$) 6.77 (d, 2H, $^3J_{HH}$ = 8.6 Hz, Ph*H*), 6.86 (d, 2H, $^3J_{HH}$ = 8.9 Hz, Ph*H*), 7.27 (m, 2H, Ph*H*), 7.63 (d, 2H, $^3J_{HH}$ = 8.9 Hz, Ph*H*). $^{13}$C NMR ($CDCl_3$, 75 MHz): $\delta$ (ppm) = 19.1, 19.7 (CH(*C*H$_3$)$_2$), 27.1 (*C*H($CH_3$)$_2$), 40.8 (*C*H$_2$NH$_2$), 47.6 (N*C*H$_2$Ph), 55.5 (PhO*C*H$_3$), 63.6 (NHCO*C*H), 67.4 (PhO*C*H$_2$), 69.6, 70.0, 70.2, 70.5, 70.6 (O*C*H$_2$*C*H$_2$O), 114.0, 114.1 (Ph*C*H), 129.3 (q-Ph*C*CH$_2$), 129.5, 130.3 (Ph*C*H), 132.2 (q-Ph*C*SO$_2$), 157.9, 162.7 (qPh*C*O), 166.7 (*C*ONHOH). HRMS (ES$^+$): calcd. ($C_{27}H_{41}N_3O_9SH$) = 584.2636; found = 584.2635.

**Fluorochrome Conjugation.** The amino-functionalized derivative 10 (1.0 mg, 1.71 $\mu$mol) was dissolved in 400 $\mu$L of dry dimethylformamide provided with 10 $\mu$L of triethylamine. To this solution, Cy5.5 NHS ester (Amersham Bioscience) (1 mg, 0.9 $\mu$mol) was added. The reaction mixture was vortexed for 2 h at room temperature in the dark. Purification of the Cy5.5-labeled derivative **6** was performed by gradient-HPLC using a Knauer system with two K-1800 pumps, an S-2500 UV detector, and a RP-HPLC Nucleosil 100−5 $C_{18}$ column (250 mm × 4.6 mm). Eluent A was water (0.1% TFA). Eluent B was acetonitrile (0.1% TFA). The gradient was from 99% A to 40% A over 19 min, holding for 5 min, and back to 99% in 1 min at a flow rate of 5.5 mL/min, and detection was at $\lambda$ = 254 nm. The appropriate fractions ($t_R$ = 14.5 min) were collected, lyophilized, redissolved in 1 mL of water, and finally stored at

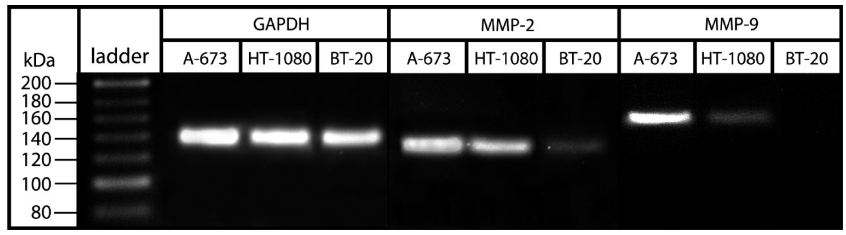


**Figure 1.** qRT-PCR was performed with primer pairs listed in Table 3, specific for MMP-2 and MMP-9, and normalized to the housekeeping gene GAPDH. After calculation of the RER for A-673, HT-1080, and BT-20, the amplified qRT-PCR products (GAPDH, 141 bp; MMP-2, 128 bp; and MMP-9, 160 bp) were analyzed by 2% gel electrophoresis.

−20 °C. The average content of **11** was 0.39 ± 0.02 μmol/mL (≈ 43%) as determined by fluorometer measurements with $\lambda_{abs}$ = 678 nm and $\varepsilon_{678}$ = 250000 $M^{-1}cm^{-1}$. MS ($ES^-$): *m/e* = 483.6 (100%), 484.0, 484.3, 484.6, 485.0 $[M]^{3-}$; 725.8, 726.3, 726.7, 727.4 $[M + H]^{2-}$.

**Cell Culture.** Three human carcinoma cell lines, purchased from ATCC (Manassas, VA, U.S.A.), were cultivated in the following media: fibrosarcoma HT-1080 (CCL-121) in RPMI-1640, mamma carcinoma BT-20 (HTB-19), and rhabdomyosarcoma A-673 (CRL-1598) in DMEM. Media (Invitrogen Corporation, San Diego, CA) were supplemented with 10% fetal calf serum (FCS), 1% penicillin and streptomycin (Biochrom AG, Berlin, Germany), 2 mM L-glutamine (Gibco BRL), and 13.5 mM sodium bicarbonate when using A-673 cells. Cells were grown routinely in T75 flasks, incubated at 37 °C in a 5% $CO_2$ humidified air atmosphere until the cultures were confluent (80−100%); medium was changed every 3−4 days. Cells were incubated with trypsin/EDTA, and cell numbers were determined in triplicate, counting only the viable cells able to exclude trypan blue (Sigma-Aldrich Chemie GmbH, Munich, Germany). For zymography, 107 cells were washed three times in serum-free medium and incubated in 3 mL of freshly FCS-free medium. After an incubation time of 48 h, the supernatant was collected and stored at −20 °C. For RNA isolation, 107 cells were incubated in FCS-containing media for further 24 h and washed with Dulbecco's phosphate-buffered saline (D-PBS) (Gibco BRL). Ten milliliters of medium was added to adherent cells, which were removed with a cell scraper and harvested by centrifugation (7 min, 1800*g*).

**RNA Isolation and cDNA Synthesis.** Total RNA was isolated from harvested cells (see above) using the PureLink Microto-Midi Total RNA Purification System (Invitrogen GmbH, Karlsruhe, Germany) according to the manufacturer's instructions with minor modifications. To remove possible genomic DNA contaminations, a DNase I digestion step was included between the washing steps. A reaction mix, consisting of OBI DNase I digestion buffer and RNase-free DNase I (20 units/μL), was added directly to the surface of the HiBind spin column for 15 min at room temperature. RNA was eluted with RNase-free DEPC-treated water and stored at −86 °C until use. The RNA quality was assessed on a 1% agarose gel, and its concentration was determined by UV spectroscopy at 260/280 nm with a NanoDrop photometer (Peqleb GmbH, Erlangen, Germany). First-strand cDNA was synthesized in a 20 μL reverse transciptase reaction mixture using the RevertAid First Strand cDNA Synthesis Kit (MBI Fermentas, St. Leon-Roth, Germany). Two micrograms of total RNA was denatured at 65 °C for 10 min and subsequently placed on ice. The no-template (NT)-control contained DEPC-treated water instead of RNA. Then, 5× reaction buffer, 1 mM of each nucleotide triphosphate, 20 units of RiboLock ribonuclease inhibitor, and 0.5 μg Oligo-(dT)18 primer were added and incubated at 25 °C for 5 min. After the addition of 200 units of RevertAid M-MuLV reverse transcriptase, the reaction mixtures were incubated according to the supplier's instructions. The no-reverse-transcription (NRT)-control contained DEPC-treated water instead of reverse transcriptase. Synthesized cDNA, the NT-, and NRT-control were stored at −20 °C until use.

**Quantitative RT-PCR.** All quantitative real-time polymerase chain reactions (qRT-PCR) were performed in a total volume of 20 μL, containing 5 μL of synthesized cDNA (or NTC or NRTC), 1 μL of SYBR Green I (1:600 diluted in DMSO) (Biozym Scientific GmbH, Oldendorf, Germany), 0.2 mM of each nucleotide triphosphate, 1× PCR-buffer, 50 μM of each primer (see Table 3), 1 mM $MgCl_2$, and 2.5 units of Taq DNA polymerase (New England Biolabs, Frankfurt a. M., Germany). To assess the accuracy of the procedures, triplicate aliquots of total RNA were used to produce cDNA in parallel reactions. QRT-PCR was accomplished using the Eppendorf Mastercycler EP Gradient (Eppendorf AG, Hamburg, Germany). The cycle conditions consisted of an initial step at 95 °C for 10 min followed by an amplification program for 40 cycles of 15 s at 95 °C, 30 s at 60 °C, 30 s at 72 °C, and 15 s at 78 °C with fluorescence acquisition. To distinguish primer dimers from the specific amplicon, the amplification program was followed immediately by a melting program consisting of 1 min at 95 °C, 1 min at 65 °C, and a gradual increase to 90 °C at a rate of 0.5 °C per second with fluorescence acquisition at each temperature transition. Linearity over the 20- to 40-cycle range and similar primer efficiencies were established by standard dilution curves (data not shown). The relative expression level of the target genes MMP-2 and -9 was normalized on the expression level of the internal housekeeping gene glycerinaldehyde-3-phosphate-dehydrogenase (GAPDH). All threshold cycle (*Ct*) values were determined in triplicate and obtained from the Eppendorf Mastercycler EP Gradient software. The relative expression ratio (RER) was determined with the comparative delta *Ct* (Δ*Ct*) method in addition to the kinetic PCR efficiency correction, using the relative expression software tool (REST). Amplified qRT-PCR products were separated by 2% agarose gel electrophoresis (Biozym Scientific GmbH, Oldendorf, Germany), stained with ethidium bromide, and visualized by UV transillumination. Fragment sizes were determined using the O'RangeRulerTM 20-bp DNA ladder (MBI Ferments, St. Leon-Rot, Germany).

**Zymography.** Gelatin zymography was performed in a sodium dodecyl sulfate (SDS)−polyacrylamide electrophoretic gel (PAGE) as described previously with minor modifications (*27*). Protein concentrations of collected FCS-free cell supernatants were derived with a Quant-iTTM Protein Assay Kit, using the Qubit fluorometer (Invitrogen GmbH, Karlsruhe, Germany). Thirty micrograms of total protein of each sample was mixed with (4×) SDS sample buffer without reducing agent and added to a 5% stacking and 7% separating SDS gel (containing 0.85 g/L gelatin). Positive controls included the following recombinant human enzymes: pro-MMP-2 (R & D Systems GmbH, Wiesbaden, Germany), active MMP-2 (Calbiochem, Wiesbaden, Germany), and pro/active MMP-9 (Sigma-Aldrich Chemie GmbH, Munich, Germany); the protein weight marker Precision Plus Dual Color (Bio-Rad Laboratories GmbH,

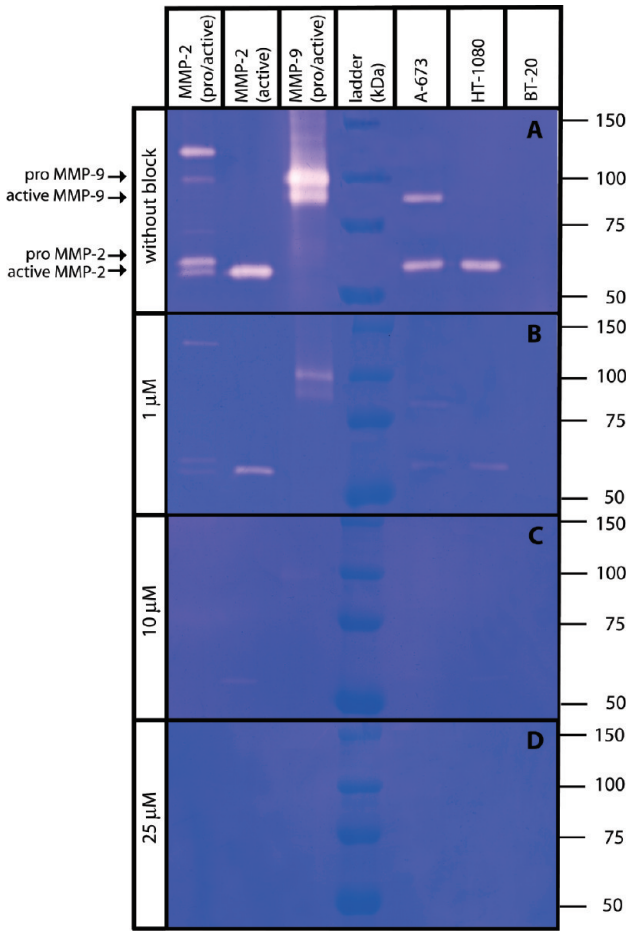


**Figure 2.** Gelatinolytic activities of purified MMP-2 (pro-form, 72 kDa; active form, 64 kDa) and MMP-9 (pro-form, 92 kDa; active form, 84 kDa) as well as that of collected supernatants of A-673, HT-1080, and BT-20 cells were assessed by zymography (A). Zymograms incubated overnight at 37 °C in buffers with varying concentrations of the unlabeled probe **10** show significant inhibition of MMP-2 and -9 by **10** (B−D). MMP-2 and -9 activities of purified enzymes and supernatants were completely inhibited by CGS concentrations ≥25 $\mu$M (D).

München, Germany) was also used. Gels were run for 120 min at 130 V and 4 °C in Tris-glycine SDS running buffer until the bromophenol blue front reached the bottom of the gel. After electrophoresis, the gels were washed with distilled water containing 2.5% Triton X-100 (30 min, room temperature) to renature proteins in the gel by the removal of SDS. Subsequently, the gels were incubated overnight at 37 °C with gentle shaking in incubation buffer (50 mM Tris-HCl at pH 7.8 and 10 mM $CaCl_2$). The incubation buffer contained 0 $\mu$M, 1 $\mu$M, 10 $\mu$M, or 25 $\mu$M unlabeled CGS-probe **10**. Zymograms were successively stained/destained with 1% Coomassie Brillant Blue G-250 dissolved in 10% ethanol and 5% acetic acid at room temperature for 120 min. Enzymatic activity was visualized through negative staining with Coomassie Brilliant Blue R-250 (Bio-Rad Laboratories GmbH, München, Germany). MMP-2/-9 activity was visible as clear zones of gelatin degradation against a dark blue background of stained gelatin. All gels were run under identical conditions with the same batch of reagents.

**Routine Cryostat Sections and Fluorescence Microscopy.** Three million cancer cells were injected subcutaneously into 7−9-week-old nude mice (nu/nu, Charles River, Germany). For in situ zymography and in vitro fluorescence binding assays, tumors with a size of approximately 7 × 10 mm were dissected, embedded into Tissue Freezing Medium (Leica Instruments, Nussloch, Germany), rapidly frozen by 2-methyl-butanol with cooled liquid nitrogen, and stored at −86 °C for sectioning. Embedded tumors were cut into 8 $\mu$m sections using a cryostat (Leica, Wetzler, Germany). For fluorescence microscopy, a Nikon TE 2000-S microscope (Tokyo, Japan) was employed, equipped with epifluorescence optics (AHF Analysentechnik AG, Tübingen, Germany). Images were recorded with a Nikon DXM1200F camera, using the NIS-Elements BR 2.30 software (Nikon, Tokyo, Japan). Fluorescence images, which had to be compared, were captured at identical illumination conditions with identical exposure time and system settings for digital image processing.

**In Vitro Fluorescence Binding Assay and in Situ Zymography.** Two hundred eighty picomoles of CGS-Cy5.5 (**11**), diluted in D-PBS (Gibco BRL), was given on unfixed air-dried cryostat sections and incubated, light protected, for 45 min at room temperature. Slides were washed in PBS (3 × 5 min) and air-dried for 5 min. Afterward, gelatinolytic activity of these cryostat sections was demonstrated using FITC-labeled dye-quenched (DQ)-gelatin, provided with the EnzCheck Gelatinase Assay Kit (EnzChek; Molecular Probes, Leiden, The Netherlands), as described previously with minor modifications (*26*). The DQ-gelatin, a specific enzymatic substrate detectable by fluorescence microscopy, is brought into close contact with cryostat sections of unfixed tissue. Proteolysis by gelatinases, such as MMP-2 and -9, yields cleaved gelatin-FITC peptides that are fluorescent so that green fluorescence indicates sites with gelatinolytic activity in tissue. At first, 1% low melting temperature agarose (Biozym Scientific GmbH, Oldendorf, Germany) was melted in D-PBS and cooled down to 37 °C, and DQ-gelatin (1 mg/mL) was added (1:200). Subsequently, a drop of the agarose−gelatin mixture was given to A-673 or BT-20 cryostat sections. All slides were incubated and light protected, at room temperature for 45 min. At the end of the incubation period, the DQ-gelatin was removed, and without fixation or wash steps, a drop of Fluoromont-GTM (Biozol Diagnostica GmbH, Eching, Germany) and a coverslip were added. Cleavage of DQ-gelatin was localized and photographed by fluorescence microscopy (emission, 535 nm; and excitation, 480 nm). Binding of CGS-Cy5.5 (**11**) to A-673 and BT-20 cryostat sections was assessed by emission of 700 nm and excitation of 620 nm.

## RESULTS AND DISCUSSION

Since MMPs are involved in the regulation of the tumor microenvironment as well as expressed and activated in many types of human cancers, this distinct enzyme class appears to be a relevant molecular target for imaging of cancer. (*11*) MMP-2 and -9 are most consistently detected in malignant tissues in which they are associated with tumor aggressiveness, metastatic potential, and poor clinical prognosis *(12, 13).*

**Chemistry.** The PEGylated benzyl derivative **5** was prepared as illustrated in Scheme 2. Mesylation of tetraethylene glycol and subsequent monosubstitution with sodium azide on a large scale gave the PEGylated azide derivative **1** in a satisfactory yield. Nucleophilic substitution of the mesyl moiety with 4-hydroxybenzaldehyde and subsequent reduc-

**Scheme 2. Synthesis of the PEG-spacer 5**[a]

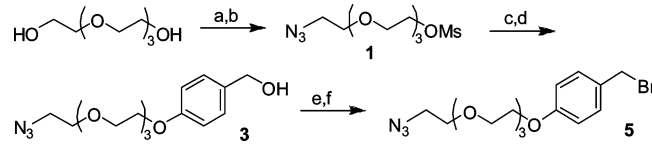


[a] (a) MsCl, $NEt_3$, $CH_2Cl_2$ (85%); (b) $NaN_3$, $CH_3CN$ (36%); (c) 4-hydroxy-benzaldehyde, $Cs_2CO_3$, DMF (75%); (d) $NaBH_4$, MeOH (89%); (e) $(TFA)_2O$, THF (95%); (f) LiBr, THF (87%).

**Scheme 3. Synthesis of the CGS-Cy5.5 11**[a]

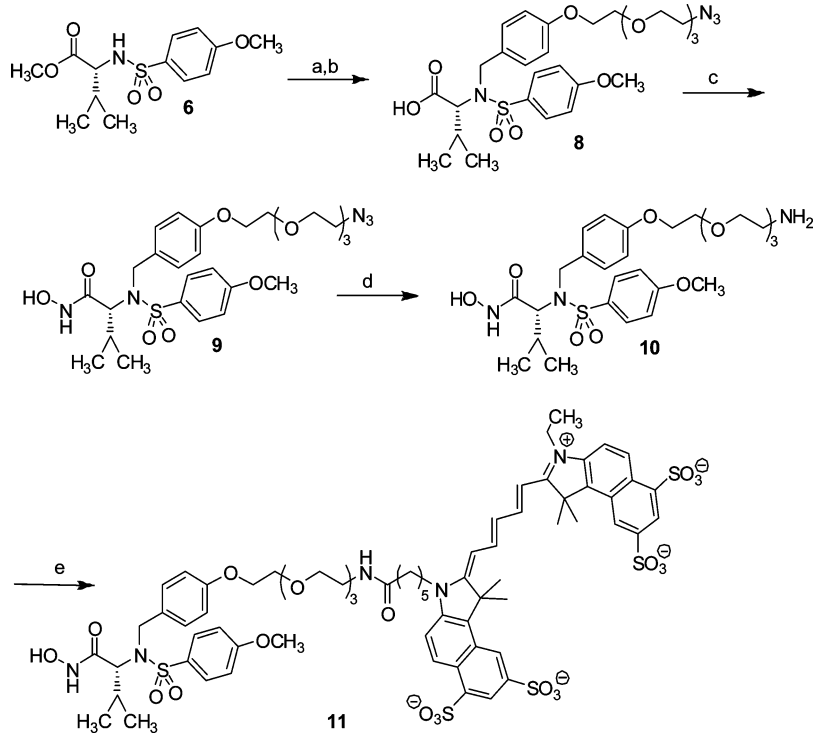


[a] (a) 5, $K_2CO_3$, butanone (73%); (b) LiOH, THF/MeOH/$H_2O$ 8/1/1 (78%); (c) (1) *N*-hydroxy-2-pyridone, 2-morpholinoethylisocyanide, TMSO-$NH_2$, $CH_2Cl_2$; (2) aq. $NaHCO_3$ (51%); (d) $PPh_3$, $H_2O$, THF (47%); Cy5.5 NHS-ester, $NEt_3$, DMF (43%).

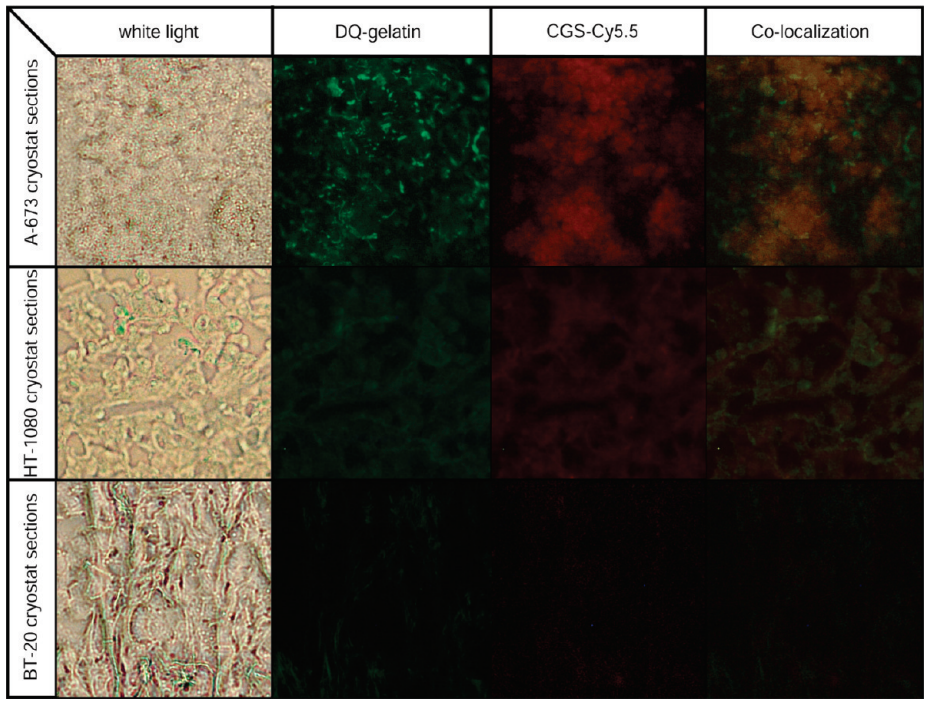


**Figure 3.** Gelatinolytic activity of A-673 (top), HT1080 (middle), and BT-20 (bottom) cryostat tumor sections was assessed by in situ zymography using FITC-labeled dye-quenched (DQ)-gelatin. In tissues with gelatinolytic activity, the DQ-gelatin was cleaved by MMP-2/-9 and resulted in green fluorescent signals. Binding of CGS-Cy5.5 (**11**) to MMP-2/-9 containing cryostat sections was demonstrated in an in vitro fluorescence binding assay. Incubation of the tumor sections with CGS-Cy5.5 resulted in high binding to A-673 sections (intense Cy5.5-based red fluorescence), a moderate binding to HT1080 sections, and low binding to BT-20 sections (low red fluorescence)). Additionally, FITC- and CGS-Cy5.5-based fluorescence was colocalized.

tion with sodium borhydride yielded the PEGylated benzyl alcohol **3**, which was converted into the benzyl bromide **5** in two steps (*14*).

On the basis of the known sulfonamide **6**, the secondary amine was benzylated and the ester hydrolyzed under mild conditions with lithium hydroxide in a THF/MeOH/water mixture (Scheme 3) Carboxylic acid **8** was directly converted into hydroxamic acid **9** with a silyl protected hydroxylamine and subsequent basic hydrolysis (*15*). For labeling with the NHS-ester of the commercially available cyanine dye Cy5.5, it

**Table 1. MMP Inhibition Potencies of the CGS-Derivatives 9, 10, and 11 for Different MMPs Expressed in $IC_{50}$ Values**

| | $IC_{50}$ [$\mu$M][a] | | | | | | | |
|---|---|---|---|---|---|---|---|---|
| Cpd | MMP-1 | MMP-2 | MMP-3 | MMP-8 | MMP-9 | MMP-13 | *c* log *D*[b] | *c* log *P*[b] |
| **9** | 0.300 ± 0.052 | 0.087 ± 0.020 | 0.058 ± 0.01 | 0.024 ± 0.005 | 0.036 ± 0.007 | 0.190 ± 0.027 | 2.96 | 2.96 |
| **10** | 0.034 ± 0.002 | 0.047 ± 0.005 | 0.007 ± 0.001 | 0.004 ± 0.001 | 0.065 ± 0.017 | 0.191 ± 0.010 | 0.37 | 2.10 |
| **11** | n.d.[c] | 16 ± 4 | n.d.[c] | n.d.[c] | 10 ± 0.7 | n.d.[c] | n.c.[d] | n.c.[d] |

[a] Values are the mean ± SD of three assays. [b] log *D* and log *P* values calculated by ACD/log *D* Suite at physiological pH. [c] Not determined. [d] Not calculated.

was necessary to reduce the azide function by a Staudinger reduction to get the precursor **10** in good yields.

The amino functionalized compound **10** was used for the conjugation of Cy5.5. The reaction was carried out in dry DMF with triethyl amine as the base (Scheme 3). Conjugate **11** was purified by reversed phase HPLC on an analytical column by collection of the appropriate fractions. After lyophilization and redissolving in PBS, the sample showed a purity of >97% (HPLC). The labeled ligand was verified by mass spectrometry with a triple negative charged ion emerging at 100% intensity.

With a molecular mass of 1,45 kDa, the resulting photoprobe belongs to the class of small molecule tracers. We and other groups are engaged in the development of MMP-targeted nonpeptide radiotracers for the in vivo detection of activated MMPs by positron emission tomography (PET) and single photon emission computed tomography (SPECT) (*16*−*20*). Recently, we successfully transferred the tracer concept to the optical imaging (OI) approach (*22*). A major advantage of OI is the opportunity to directly correlate signals in vivo with high resolution ex vivo techniques (e.g., fluorescence microscopy). A direct coregistration of biological expression patterns and the biodistribution of the tracer are thus feasible (see Figure 3). Moreover, the stability of the label and the lack of signal decay allow measurements over several days. With respect to clinical applications, small targeted probes could potentially allow endoscopic or laparoscopic tumor detection with high signal-to-noise ratios (SNRs). Imaging in the near-infrared spectrum ($\lambda$ = 650−950 nm) shows very efficient tissue penetration as the absorption by water and hemoglobin is relatively low (diagnostic window) (*21, 22*). Moreover, the tracer's excitation and emission spectra were identical to that of the Cy5.5 dye (ex, 678 nm; em, 692 nm).

**Enzyme Studies in Vitro.** A synthetic fluorogenic broad-spectrum MMP substrate was used in vitro to measure the activity of recombinant active human MMP-2 and -9 in the presence and absence of the unlabeled CGS **9** and **10**. The resulting inhibition potencies for several MMPs were determined as $IC_{50}$ values and calculated from a nonlinear regression curve fit of the concentration-dependent reaction rates. This fluorogenic enzymatic activity assay yielded binding affinities of **9** and **10** to MMP-2 and -9 in the nanomolar range (Table 1).

**MMP-2 and -9 Transcription, Translation, and Activity Tests.** Three human cancer cell lines (rhabdomyosarcoma A-673, fibrosarcoma HT-1080 and breast carcinoma BT-20) were characterized regarding their genomic, proteomic, and functional MMP-2 and -9 expression levels. Cells were analyzed by quantitative real-time-PCR (qRT-PCR), secreted MMP proteins of collected supernatants were detected by Western blot analysis (data not shown), and MMP-2/-9 activities were verified by zymography.

In qRT-PCR analysis, the mRNA expression of the target genes MMP-2 and -9 was normalized by the internal housekeeping gene GAPDH since all three cancer cell lines (A-673, HT-1080, and BT-20) revealed nearly identical GAPDH mRNA levels. Using the software tool REST (*23*), the relative expression ratios (RER) of the target genes were determined as shown in Table 2. After determination of the RERs, amplified qRT-PCR products were analyzed in a 2% gelelectrophoresis as shown in Figure 1. Highest MMP-2 and -9 mRNA levels could be obtained for A-673, which therefore represented a MMP-2 and -9 positive cell line for the study of the binding affinity of CGS-Cy5.5 **11** to secreted gelatinases. HT-1080 cells showed high MMP-2 levels but weak MMP-9 mRNA levels. BT-20 cells expressed MMP-2 in very low amounts as compared to A-673 and HT-1080 cells. The MMP-9 mRNA level of BT-20 cells was lower than detectable levels; BT-20, therefore, was used as a cell line with very low gelatinase activity in our study.

**Table 2. MMP-2 and -9 Expressions of the Carcinoma Cell Line A-673, HT-1080, and BT-20 Were Analyzed by qRT-PCR Analysis[a]**

| | A-673 | HT-1080 | BT-20 |
|---|---|---|---|
| MMP-2 RER | 23.0 | 12.7 | 1.0 |
| MMP-9 RER | 33.0 | 1.0 | 0 |

[a] The relative expression ratios (RER) for the target genes MMP-2 and -9 were determined by the software tool REST.

**Table 3. Oligonucleotides Used As Primers**

| oligonucleotides | 5′ → 3′-sequence | fragment size (bp) |
|---|---|---|
| GAPDH-for | CATTGCCCTCAACGACCAC | 141 |
| GAPDH-rev | CCTCTTGTGCTCTTGCTGGG | |
| MMP-2-for | GGAATGCCATCCCCGATAA | 128 |
| MMP-2-rev | TGCTTCCAAACTTCACGCTCT | |
| MMP-9-for | CCAAGTGGGCTACGTGACCTA | 160 |
| MMP-9-rev | CCTCCCTTTCCTCCAGAACAG | |

Furthermore, gelatinolytic activities of collected supernatants from A-673, HT-1080, and BT-20 cells were analyzed by gelatin zymography. Purified MMP-2 and -9 (pro-/active forms) were used as controls (Figure 2A). Two prominent bands of gelatinolytic activity could be observed for the MMP-9 standard: the upper band exhibits the pro-form (92 kDa) and the lower band the active form (84 kDa). Purified pro-MMP-2 (72 kDa) and active MMP-2 (64 kDa) were identified accordingly. Furthermore, active MMP-2 was secreted by A-673 and HT-1080 cells. Active MMP-9 could only be detected in the supernatant of A-673 cells. Supernatants of BT-20 cells showed no detectable MMP-2 and -9 activities in zymography (Figure 2A). MMP-2 and -9 activities of the supernatants, analyzed with zymography, nicely correspond to the determined MMP-2-/9 relative expression ratios (RER) of the cells, analyzed by qRT-PCR. In following experiments, zymograms were incubated in buffers containing different amounts of the nonlabeled probe **10**. Varying the concentrations of the nonlabeled probe from 1 $\mu$M to 25 $\mu$M (Figure 2B−D) demonstrated its inhibition potential. Gelatinolytic activities of purified enzymes and cell supernatants were completely inhibited in the presence of 25 $\mu$M unlabeled CGS **10** as shown in Figure 2D, indicating efficient inhibition of MMP-2 and -9 by the probe.

Additionally, MMP-2 and -9 proteins in the collected supernatants were assessed by Western blotting with polyclonal antibodies, which recognize the latent and active MMP-2 and -9 forms. Western blot analysis and purified enzymes confirmed the results obtained with zymography (data not shown (*24*)).

**Cellular Fluorescence MMP-Binding Assay of the Cy5.5-Labeled CGS (11) Using Cryostat Sections in Vitro.** In situ zymography was used to proof high (A-673), weak (HT1080),

and low (BT-20) MMP-2 and -9 activities of respective tumor cryostat sections. Gelatinolytic activity was visualized in thin tissue sections by FITC-labeled dye-quenched (DQ)-gelatin, resulting in green fluorescence only in the case of enzymatic conversion. As expected, high extracellular and cellular green fluorescence was observed in the majority of regions of A-673 tumor sections (Figure 3) proving high MMP-2 and -9 activities of A-673 tumors suggested by the previous qRT-PCR and zymography experiments. Accordingly, BT-20 sections showed very low FITC-based fluorescence signals and only weak green fluorescence at the tumor border (Figure 3). In the fluorescence binding assay, MMP-2 and -9 containing A-673 tumor cryostat sections were treated with PBS containing 280 pmol of CGS-Cy5.5 **11**. High Cy5.5-based red fluorescence was obtained for A-673 sections as demonstrated in Figure 3. These results suggest high binding affinity of the labeled probe to gelatinases, secreted by the A673 tumor. In contrast, incubation of BT-20 sections showed only weak red fluorescence and revealed low binding of CGS-Cy5.5 **11** (Figure 3). CGS-Cy5.5- and FITC-based fluorescence signals were found colocalized, and further proof that activated MMPs can be detected with the newly developed photoprobe.

Alternative imaging approaches have been previously described in the literature (*25*). Large self-quenched molecules, e.g., allowed one to assess MMP expression in vivo via enzymatic activation of the probe. While this approach is a highly sensitive method for the detection of MMP activity, large molecule size (app. 400−500 kDa) and thus long blood half-life may be undesirable for translational imaging approaches.

## CONCLUSIONS

The aim of this work was the development of a nonpeptide MMP inhibitor for optical imaging of MMP-2 and -9 activities. We have chosen CGS 25966 as the lead structure and developed a route for the synthesis of an amino-PEG-derivatized compound that can be used for the conjugation of common amino-reactive fluorescent markers such as Cy5.5. Thus, we obtained a near-infrared fluorescent photoprobe for the imaging of MMP-2 and -9. Using techniques such as qRT-PCR and zymography, the MMP-2 and -9 expressions of three human cancer cell lines was analyzed. The rhabdomyosarcoma cell line A-673 showed high MMP-2 and -9 levels, whereas the fibrosarcoma cell line HT-1080 exhibits lower levels and the breast carcinoma cell line BT-20 only marginal levels of MMP-2. MMP-2 and -9 activities of the three cell supernatants were verified by zymography. In subsequent blocking experiments, zymograms were incubated with different concentrations of unlabeled CGS **10**. Incubation with $\geq 25$ $\mu$M unlabeled inhibitor revealed efficient binding and inhibition of MMP-2 and -9 activities. Additionally, gelatinolytic activity of A-673 and BT-20 cryostat sections was determined by in situ zymography using the DQ-gelatin technique. High binding affinity of CGS-Cy 5.5 **11** to MMP-2 and -9 containing A-673 tumor cryostat sections was demonstrated in an in vitro fluorescence binding assay. Thus, MMP-2 and -9 imaging with the fluorescent labeled probe **11** is feasible and should further be developed toward a molecular imaging approach to monitor disease processes such as invasion, metastasis, and angiogenesis in cancer in vivo being associated with activated MMP-2 and -9.

## ACKNOWLEDGMENT

This work was supported by the Deutsche Forschungsgemeinschaft (SFB 656 projects A2/A4), the European Union Community (IP sixth framework; grant no. LSHG-CT-2003-503259 (Mol. Img) and MoldDiag-Paca LSHB- CT-2006-018771), the Interdisziplinary Centre of Clinical Research (FG3), and the European Institute for Molecular Imaging (EIMI). Thanks are due to Wiebke Gottschlich, Ulla Römer, and Sandra Schröer for technical assistance, and Professor Dr. H. Luftmann at the Organic Chemistry Department of the WWU Münster for mass spectrometry.

## LITERATURE CITED

(1) Skiles, J. W., Gonnella, N. C., and Jeng, A. Y. (2004) The design, structure, and clinical update of small molecular weight matrix metalloproteinase inhibitors. *Curr. Med. Chem. 11*, 2911–2977.

(2) Tayebjee, M. H., Lip, G. Y. H., and MacFadyen, R. J. (2005) Matrix metalloproteinases in coronary artery disease: clinical and therapeutic implications and pathological significance. *Curr. Med. Chem. 12*, 917–925.

(3) Beaudeux, J. L., Giral, P., Bruckert, E., Foglietti, M. J., and Chapman, M. J. (2004) Matrix metalloproteinases, inflammation and atherosclerosis: therapeutic perspectives. *Clin. Chem. Lab. Med. 42*, 121–131.

(4) Whittaker, M., and Ayscough, A. (2000) Matrix metalloproteinases and their inhibitors - current status and future challenges. *Cell Transm. 17*, 3–14.

(5) Borkakoti, N. (2000) Structural studies of matrix metalloproteinases. *J. Mol. Med. 7*, 261–268.

(6) Stamenkovic, I. (2003) Extracellular matrix remodelling: the role of matrix metalloproteinases. *J. Pathol. 200*, 448–464.

(7) Galis, Z. S., and Khatri, J. J. (2002) Matrix metalloproteinases in vascular remodeling and atherogenesis: the good, the bad, and the ugly. *Circ. Res. 90*, 251–62.

(8) George, S. J. (2000) Therapeutic potential of matrix metalloproteinase inhibitors in atherosclerosis. *Exp. Opin. Invest. Drugs 9*, 993–1007.

(9) Katiyar, S. K. (2006) Matrix metalloproteinases in cancer metastasis: molecular targets for prostate cancer prevention by green tea polyphenols and grape seed proanthocyanidins. *Endocr., Metab. Immune Disord.: Drug Targets 6*, 17–24.

(10) Fridman, R. (2006) Metalloproteinases and cancer. *Cancer Metastasis Rev. 25*, 7–8.

(11) Vihinen, P., Ala-aho, R., and Kahari, V. M. (2005) Matrix metalloproteinases as therapeutic targets in cancer. *Curr. Cancer Drug Targets 5*, 203–20.

(12) Egeblad, M., and Werb, Z. (2002) New functions for the matrix metalloproteinases in cancer progression. *Nat. Rev. Cancer 2*, 161–74.

(13) Fingleton, B. (2003) Matrix metalloproteinase inhibitors for cancer therapy: the current situation and future prospects. *Expert Opin. Ther. Targets 7*, 385–397.

(14) Kopka, K., Faust, A., Keul, P., Wagner, S., Breyholz, H.-J., Höltke, C., Schober, O., Schäfers, M., and Levkau, B. (2006) 5-pyrrolidinylsulfonyl isatins as a potential tool for the molecular imaging of caspases in apoptosis. *J. Med. Chem. 49*, 6704–6715.

(15) Hilpert, H. (2001) Practical approaches to the matrix metalloproteinase inhibitor Trocade® (Ro 32-3555) and to the TNF-α converting enzyme inhibitor Ro 32-7315. *Tetrahedron 57*, 7675–7683. (a) Kopka, K., Breyholz, H.-J., Wagner, S., Law, M. P., Riemann, B., Schröer, S., Trub, M., Guilbert, B., Levkau, B., Schober, O., and Schäfers, M. (2004) Synthesis and preliminary biological evaluation of new radioiodinated MMP inhibitors for imaging MMP activity in vivo. *Nucl. Med. Biol. 31*, 257–267.

(16) Schäfers, M., Riemann, B., Kopka, K., Breyholz, H.-J., Wagner, S., Schäfers, K. P., Law, M. P., Schober, O., and Levkau, B. (2004) Scintigraphic imaging of matrix metalloproteinase activity in the arterial wall *in vivo*. *Circulation 109*, 2554–2559.

(17) Breyholz, H.-J., Wagner, S., Levkau, B., Schober, O., Schäfers, M., and Kopka, K. (2007) A 18F-radiolabeled analogue of CGS 27023A as a potential agent for assessment of matrix-metalloproteinase activity in vivo. *Q. J. Nucl. Med. Mol. Imaging 51*, 24–32.

(18) Wagner, S., Breyholz, H.-J., Law, M. P., Faust, A., Holtke, C., Schroer, S., Haufe, G., Levkau, B., Schober, O., Schafers, M., and Kopka, K. (2007) Novel fluorinated derivatives of the broad-spectrum MMP inhibitors N-hydroxy-2(*R*)-[[(4-methoxyphenyl)sulfonyl](benzyl)- and (3-picolyl)-amino]-3-methyl-butanamide as potential tools for the molecular imaging of activated MMPs with PET. *J. Med. Chem. 50*, 5752–5764.

(19) Su, H., Spinale, F. G., Dobrucki, L. W., Song, J., Hua, J., Sweterlitsch, S., Dione, D. P., Cavaliere, P., Chow, C., Bourke, B. N., Hu, X. Y., Azure, M., Yalamanchili, P., Liu, R., Cheesman, E. H., Robinson, S., Edwards, D. S., and Sinusas, A. J. (2005) Noninvasive targeted imaging of matrix metalloproteinase activation in a murine model of postinfarction remodeling. *Circulation 112*, 3157–3167.

(20) Chung, G., and Sinusas, A. J. (2007) Imaging of matrix metalloproteinase activation and left ventricular remodeling. *Curr. Cardiol. Rep. 9*, 136–142.

(21) Ntziachristos, V., Bremer, C., Graves, E. E., Ripoll, J., and Weissleder, R. (2002) In vivo tomographic imaging of near-infrared fluorescent probes. *Mol Imaging 1*, 82–88.

(22) Bremer, C., Ntziachristos, V., Weitkamp, B., Theilmeier, G., Heindel, W., and Weissleder, R. (2005) Optical imaging of spontaneous breast tumors using protease sensing 'smart' optical probes. *Invest. Radiol. 40*, 321–327.

(23) Pfaffl, M. W., Horgan, G. W., and Dempfle, L. (2002) Relative expression software tool (REST) for group-wise comparison and statistical analysis of relative expression results in real-time PCR. *Nucleic Acids Res. 26*, 509–515.

(24) Faust, A., Waschkau, B., Waldeck, J., Höltke, C., Breyholz, H.-J., Wagner, S., Kopka, K., Heindel, W., Schäfers, M., and Bremer, C. (2008) Synthesis and evaluation of a novel fluorescent photoprobe for imaging matrix metalloproteinases. *Bioconjugate Chem. 19*, 1001–1008.

(25) Bremer, C., Tung, C. H., and Weissleder, R. (2001) *In vivo* molecular target assessment of matrix metalloproteinase inhibition. *Nature Med. 7*, 743–748.

(26) Oh, L. Y., Larsen, P. H., Krekoski, C. A., Edwards, D. R., Donovan, F., Werb, Z., and Yong, V. W. (1999) Matrix metalloproteinase-9/gelatinase B is required for process outgrowth by oligodendrocytes. *J. Neurosci. 19*, 8464–8475.

(27) Heussen, C, and Dowdle, E. B. (1980) Electrophoretic analysis of plasminogen activators in polyacrylamide gels containing sodium dodecyl sulfate and copolymeri/ed substrates. *Anal. Biochem. 102*, 196–202.

BC8004478